Groundwater

A Comparison of Hyporheic Transport at a Cross-Vane Structure and Natural Riffle

by Samuel J. Smidt[1], Joseph A. Cullin[1], Adam S. Ward[2], Jesse Robinson[3], Margaret A. Zimmer[4], Laura K. Lautz[5], and Theodore A. Endreny[6]

Abstract

While restoring hyporheic flowpaths has been cited as a benefit to stream restoration structures, little documentation exists confirming that constructed restoration structures induce comparable hyporheic exchange to natural stream features. This study compares a stream restoration structure (cross-vane) to a natural feature (riffle) concurrently in the same stream reach using time-lapsed electrical resistivity (ER) tomography. Using this hydrogeophysical approach, we were able to quantify hyporheic extent and transport beneath the cross-vane structure and the riffle. We interpret from the geophysical data that the cross-vane and the natural riffle induced spatially and temporally unique hyporheic extent and transport, and the cross-vane created both spatially larger and temporally longer hyporheic flowpaths than the natural riffle. Tracer from the 4.67-h injection was detected along flowpaths for 4.6 h at the cross-vane and 4.2 h at the riffle. The spatial extent of the hyporheic zone at the cross-vane was 12% larger than that at the riffle. We compare ER results of this study to vertical fluxes calculated from temperature profiles and conclude significant differences in the interpretation of hyporheic transport from these different field techniques. Results of this study demonstrate a high degree of heterogeneity in transport metrics at both the cross-vane and the riffle and differences between the hyporheic flowpath networks at the two different features. Our results suggest that restoration structures may be capable of creating sufficient exchange flux and timescales of transport to achieve the same ecological functions as natural features, but engineering of the physical and biogeochemical environment may be necessary to realize these benefits.

Introduction

Hyporheic exchange underpins a host of ecosystem services and processes (e.g., Findlay 1995; Brunke and Gonser 1997; Boulton et al. 1998, 2008; Krause et al. 2011). The benefits of hyporheic exchange are primarily due to the increased contact time between stream water and the microbial communities in the hyporheic zone (e.g., Findlay 1995; Valett et al. 1996; Boulton et al. 1998), which has been linked to a host of biogeochemical processes (e.g., Battin 1999; Fellows et al. 2001; Craig et al. 2008). Given these benefits and the growing desire to restore ecosystem function in streams and rivers (e.g., Bernhardt et al. 2005), hyporheic restoration has been proposed as a management strategy for promoting healthy stream ecosystems (e.g., Bernhardt and Palmer 2007; Boulton 2007; Boulton et al. 2010; Hester and Gooseff 2010, 2011; Krause et al. 2011; Ward et al. 2011). Although there is widespread recognition of the importance of hyporheic restoration, few studies have compared natural features (the identified standard for hyporheic exchange) to artificial restoration features (the identified method for restoration). Daniluk et al. (2013) compared restored sites to natural reference sites and found that cross-vane structures (horseshoe-shaped, anthropogenic restoration structures used primarily for grade and bank stabilization by directing flow toward the center of the stream channel) at restored sites generated greater hyporheic flux than was observed at natural features. They also found that geochemical patterns at restoration structures resembled surface water whereas patterns at natural sites resembled mixing surface water and groundwater. Lautz and Fanelli (2008) also compared natural sites to restoration structures and found that changes in pore water geochemistry at a restored site were due to the restoration structure and not to the patterns seen at analogous natural sites. Gordon et al. (2013) compared cross-vane restoration structures across field sites and

[1]Department of Earth & Environmental Sciences, The University of Iowa, Iowa City, IA 52242.
[2]Corresponding author: School of Public and Environmental Affairs, Indiana University 430 MSB-II, Bloomington, IN 47405; (812) 856-4820; adamward@indiana.edu
[3]Stream Institute, Department of Civil and Environmental Engineering, University of Louisville, Louisville, KY 40206.
[4]Division of Earth and Ocean Sciences, Nicholas School of the Environment, Duke University, Durham, NC 27708.
[5]Department of Earth Sciences, Syracuse University, Syracuse, NY 13244.
[6]Department of Environmental Resources Engineering, SUNY-ESF, Syracuse, NY 13210.

Received September 2014, accepted September 2014.

doi: 10.1111/gwat.12288

found that these structures induce exchange flux at rates too rapid to promote biogeochemical processing in the hyporheic zone. Despite these comparisons, there is still a gap in our understanding of the physical transport at natural features and restoration structures and the implications for restoration design. In this study, we directly compare hyporheic zone extent and temporal patterns in solute transport along hyporheic flowpaths at a constructed cross-vane and a naturally occurring riffle.

Study of hyporheic restoration related to structure design has historically relied on the idea that the creation of a hyporheic exchange zone directly results in desired ecosystem services (i.e., ecosystem function follows form; Findlay 1995; Boulton 2007). Vidon et al. (2010) attributed the ecological benefit of hyporheic exchange to a combination of rapid reaction rates (process driven) and exchange flux (transport driven). While process and transport combine to realize an ecosystem service associated with hyporheic exchange, the functions cannot be realized in the absence of transport processes (Ward et al. 2011). As a result, hyporheic hydrodynamics are primarily defined by the flux and solute residence time along flowpaths (e.g., Boulton et al. 1998; Pinay et al. 2009) suggesting that the installation of restoration structures may not directly result in desired ecosystem services as historically anticipated.

Instead, several recent studies of restoration and natural structures have observed greater complexity regarding hyporheic zone drivers. For example, recent studies have concluded heterogeneous patchiness is an important feature that determines function (e.g., Fanelli and Lautz 2008; Gordon et al. 2013). It has also been demonstrated that disturbances to both surface (e.g., Sawyer et al. 2011) and subsurface hydraulics (Vaux 1968; Ward et al. 2011) can modify hyporheic exchange flux with implications for structure design. Gordon et al. (2013) found that subsurface transport around cross-vanes was more complex than simple conceptual models would predict, citing heterogeneity near restoration structures as the source of this complexity. Based on streambed flux and biogeochemical evidence, Gordon et al. (2013) concluded that transport near the restoration structure is too rapid to contribute to ecosystem function, but suggested secondary bedforms (e.g., pool-riffle structures downstream) are of appropriate timescales to support desired ecosystem function of stream restoration. In the context of hyporheic restoration, past studies have inferred that heterogeneity in subsurface transport processes is related to biogeochemical function (e.g., Gordon et al. 2013), but none have directly investigated these processes.

The design of restoration structures and the resulting hyporheic transport function have been successfully studied in idealized conditions including both numerical (e.g., Hester and Doyle 2008; Ward et al. 2012a) and scale-model investigations (e.g., Endreny et al. 2011; Sawyer et al. 2011; Zhou and Endreny 2013). The value of such studies is to control a host of variables to isolate a specific process or control on hyporheic exchange. However, contradictions between some studies challenge our understanding of hyporheic hydraulics (Endreny and Lautz 2012). For example, Crispell and Endreny (2009) found disagreement between models based on fluid dynamics and those based on vertical hydraulic gradients. Lautz and Ribaudo (2012) found that evidence based on diel temperature fluctuations contradicted geochemical mixing model predictions. In all of these studies, the methods employed integrate a limited suite of spatial and temporal scales and support different conceptual models of hyporheic exchange. The heterogeneity in spatial and temporal scales of hyporheic flowpaths and the methods used to observe them are critical limitations in our understanding of hyporheic transport.

Electrical resistivity (ER) tomography has emerged as a tool to minimize methodological limitations due to spatiotemporal variability in quantifying hyporheic transport processes in situ (e.g., Ward et al. 2010, 2011, 2012a, 2013a; Cardenas and Markowski 2011; Toran et al. 2012; Menichino et al. 2014). Time-series analysis of individual pixels in ER inversion images has been used to characterize transport processes in numerical models (Kemna et al. 2002), soil columns (Binley et al. 1996), and in both two-dimensional (2D) and three-dimensional (3D) scale model studies (Slater et al. 2000, 2002). More recently, Ward et al. (2014) inferred hyporheic transport processes from time-series analysis of ER images during solute tracer studies. These studies demonstrate the ability of geophysical imaging to characterize transport processes in porous media and to observe heterogeneities in transport where flowpaths intersect the ER transect.

The objective of this study is to compare hyporheic extent and the distribution of transport metrics at a constructed cross-vane and a downstream riffle. This study uses electrical geophysical tomography in conjunction with a conductive and conservative solute tracer to quantify temporal and spatial hyporheic flowpath networks associated with the compared features. Although the design of the restoration structure was neither for the goal of hyporheic restoration nor to replicate an in-stream riffle (the cross-vane was installed as a bank stabilization technique), this study provides a unique comparison of the function of a stream restoration structure and a natural feature during equivalent hydrologic settings in the same stream reach. Many past studies have suggested hyporheic restoration potential at traditional in-stream restoration structures (e.g., Hester and Doyle 2008; Hester and Gooseff 2010, 2011; Ward et al. 2011); this study tests the idea in a field setting. Comparison of the spatial and temporal extent of hyporheic exchange beneath artificial and natural structures is a requisite step to prediction of the influence of restoration on hyporheic function.

Methods

Site Description and Study Design

Figure 1 shows a cross-vane restoration structure and a riffle positioned in a highly instrumented 30 m reach of W. Branch Owego Creek in New York. The cross-vane

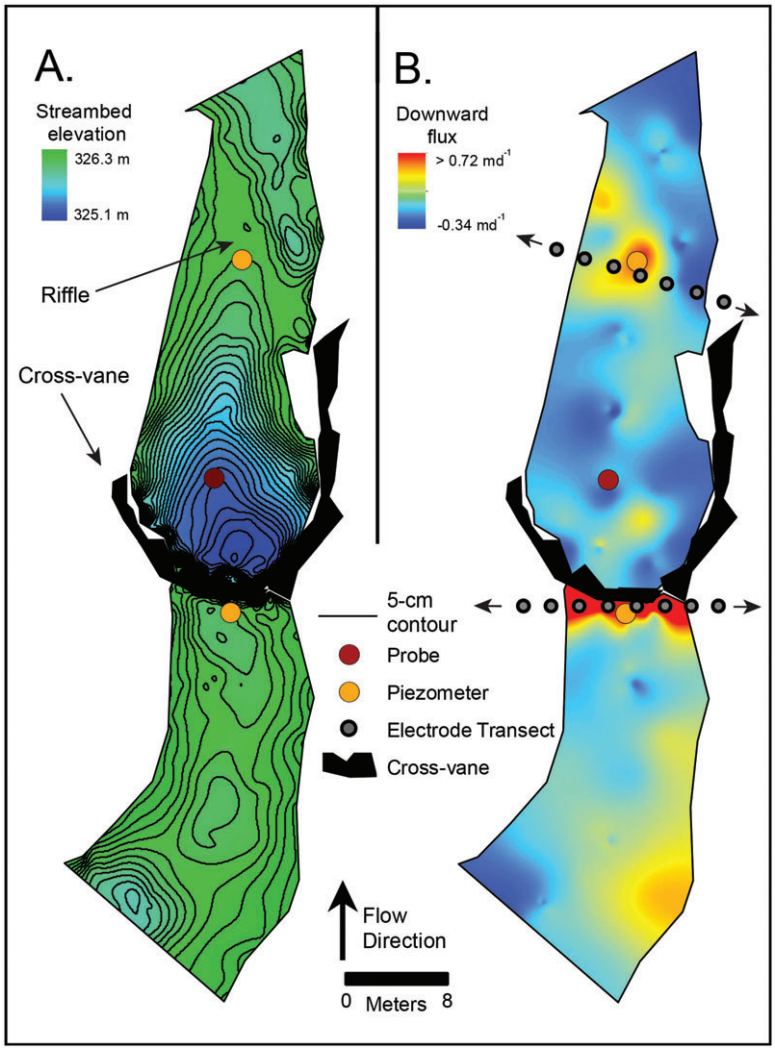

Figure 1. The cross-vane structure was located upstream of the riffle. A scour hole was located directly downstream of the cross-vane (A). Piezometers directly upstream of each feature were used to collect electrical conductivity of pore water. An in-stream conductivity probe collected electrical conductivity of surface water. Downwelling flux occurred directly upstream of the cross-vane and riffle, and upwelling flux occurred directly downstream of the two features (B). One ER transect was located directly above each feature to capture hyporheic flowpaths crossing a 2D plane perpendicular to the streambed. Figure 1 has been modified from Figures 2 and 6 from Gordon et al. 2013.

was constructed in 2006 using stone blocks and spans the 8 to 10 m wide channel and extends into the banks. Our study was conducted in 2012. The water depth was 22 cm immediately upstream of the cross-vane. A plunge pool with a depth of approximately 1.13 m was located downstream of the cross-vane. A natural riffle was located approximately 18 m downstream of the cross-vane. The riffle spanned the width of the channel and was approximately 2 m long. The head differential (i.e., the difference between the water level before and after the feature) across the cross-vane and the riffle were 17.8 and 5.5 cm, respectively. At the study site, the W. Branch Owego Creek catchment drained 74.4 km^2 and had a discharge of 260 L/s during this study. In a previous study, Gordon et al. (2013) conducted a detailed topographic survey of the study reach and estimated vertical streambed flux using temperature time series (Figure 1).

Solute Tracer Study

Sodium chloride (NaCl) was dissolved in stream water and injected at a constant rate of 4.6 L/min for 4.67 h into the stream channel 145 m (equivalent to approximately 15 wetted-channel widths) upstream of the study reach. The mixing across the stream channel was verified through measurement of stream tracer concentration at multiple locations at the upstream ER transect. The in-stream specific conductivity increased by 38% from background during the plateau of injection. The in-stream tracer was monitored as specific conductivity (temperature-corrected fluid electrical conductivity) immediately downstream of the cross-vane using a YSI MPS 556 Multimeter (YSI Inc./Xylem Inc., Yellow Springs, Ohio). Data were converted to concentration using a calibration curve constructed by dissolving known masses of NaCl dissolved in stream water. Additionally, specific conductivity was measured at 50 cm

depth below the streambed in two streambed piezometers, each of which was screened over a 5 cm length. One piezometer was located in each of the downwelling locations directly upstream of the cross-vane and the riffle (Figure 1) using EC300 probes (YSI Inc./Xylem Inc., Yellow Springs, Ohio). The piezometers were installed to validate the ER inversions conducted at each transect; water measurements from each piezometer represent an average of flowpaths that intersect the screened length. Still, these provide a useful comparison to ensure ER time series are accurately representing the solute transport processes.

Geophysical Data Collection and Inversion

Electrical resistivity tomography was used to characterize the spatial extent of hyporheic flowpaths and obtain spatially distributed time series of bulk electrical resistivity (e.g., Nyquist et al. 2010; Ward et al. 2010, 2012a; Toran et al. 2012; Menichino et al. 2014). Two 16-electrode transects were installed perpendicular to the streambed and centered on the stream channel. One transect was located immediately upstream of the cross-vane and the second at the crest of the riffle. Electrode spacing along each transect was 2 m. Electrodes on the banks were stainless steel rods of 1.5 cm diameter driven to a depth of approximately 20 cm into the floodplain soils. Electrodes in the streambed were constructed of stainless steel foil tape on a PVC rod driven to a depth of 20 cm below the streambed and connected to the geophysical equipment using copper wire (after Ward et al. 2012a). Because results are dependent upon the location of the ER transect, we placed each transect directly upstream of each feature to capture peak downwelling as observed by the vertical temperature profiling of Gordon et al. (2013) (Figure 1). Other studies have also confirmed that peak downwelling has occurred directly upstream of a feature (Hester and Doyle 2008; Hester et al. 2009; Sawyer and Cardenas 2012).

Electrical resistivity data were collected using a sequence of 305 quadrupoles (unique combinations of an electrical current pair and voltage potential pair of electrodes) at each transect. Collection time for an individual transect was approximately 3 min, and collection alternated between transects. ER data collection began prior to the tracer injection and continued until after the falling limb was observed in the piezometer network. No reciprocal data were collected in order to maximize temporal resolution of the data collection scheme (after Ward et al. 2010, 2012a; Menichino et al. 2014). ER data were collected with a SyscalPro 10-channel meter (IRIS Instruments, Orleans, France). We stacked (averaged) two voltage potential readings for each quadrupole and added a third measurement to the stack if the standard deviation as a percent of the mean was greater than 3%.

Electrical resistivity data were inverted using the research code R2 (v2.6, Generalized 2D Inversion of Resistivity Data, available at http://www.es.lancs.ac.uk/people/amb/Freeware/freeware.htm). Data collected in each set of 305 quadrupoles were assigned to a single time centered within the data collection for that set. Temporal smearing within each data set was assumed to be minimal given the speed of the collection scheme. The inversion algorithm was based on an Occam's inversion (Binley and Kemna 2005). The inversion domain was represented as a grid of 10-cm pixels, including surveyed surface topography along each transect. Electrodes were represented as point sources located at the model domain surface. We assumed an error model of 0.001 Ω absolute error in field data and a relative error of 0.5% of the observed resistance. Data were equally weighted initially with weights adjusted iteratively by the inversion. Background (pre-tracer) data were inverted starting with a homogeneous starting model of 400 Ω-m for each transect. Subsequent data were inverted on differences from the background data set using the difference inversion scheme of LaBrecque and Yang (2001). The steps of data collection and inversion follow those of several recent studies of hyporheic solute transport (e.g., Ward et al. 2012b, 2014).

Images resulting from the inversion process generate a value of bulk electrical resistance for each pixel. These data were filtered using two steps (after Ward et al. 2012a; Menichino et al. 2014). First, the diagonal of the resolution matrix (see Binley and Kemna 2005 for further details) was used to identify pixels where the inversion was able to uniquely determine at least 0.4% of a pixel's value. Next, background noise and error in the inversion process were differentiated from signal due to the solute tracer using a threshold of 5% decrease from background (pre-tracer) resistivity (i.e., changes of less than 5% were considered noise and were not interpreted). Pixels not meeting both criteria were excluded from interpretation. We emphasize here that the interpretation of geophysical images must be conducted within the context of known limitations. Geophysical images are both ill-posed (i.e., nonunique solutions are generated by the inversion process) and ill-conditioned (i.e., small data errors may lead to large model error) (Koestel et al. 2009). The inversion process also includes a number of limiting assumptions including representing a 3D field in a 2D plane which may generate some out-of-plane effects on the solutions, spatial and temporal smearing of data, and nonuniqueness of solutions to the inverse problem (for further discussion of geophysical limitations, see Slater et al. 2002; Day-Lewis et al. 2005, 2007).

Analysis of Time Series Data

Quantified metrics for in-stream, piezometer, and transect time series provide insight into the solute transport and exchange patterns underneath each feature through the comparison of summarized statistics along the stream reach. Several metrics summarizing the time series were calculated from both observed fluid conductivity time series (stream, piezometers) and the time series of pixel resistivity resulting from the inversion process. For pixel data, the decrease in electrical resistivity from background was analyzed for a single pixel time series. For in-stream and piezometer data, fluid specific

conductivity was analyzed. Times of first detection (t_{first}) and the passage of 99% of the observed signal (t_{99}) were calculated for each time series observed (after Mason et al. 2012; Ward et al. 2013a). The duration of tracer detection was calculated as

$$t_{detection} = t_{99} - t_{first} \quad (1)$$

Next, all time-series data were analyzed by calculation of temporal moments to describe advective transport, spreading, and skewness (after Gupta and Cvetkovic 2002; Schmid 2003). First, temporal data were normalized such that the total area bounded by each time series is unity, as

$$C_{norm} = \frac{C(t)}{\int_0^{t_{max}} C(t)\,dt} \quad (2)$$

where $C(t)$ is the time-series data being analyzed (decrease in resistivity for inversion pixels, increase in fluid specific conductivity for in-stream and piezometer data), C_{norm} is the normalized time series, t is time elapsed from the start of the tracer injection, and t_{max} is the last observation in the time series. Next, temporal moments (M_k) were calculated for each time series using

$$M_k = \int_0^{t_{max}} C_{norm}(t) t^k dt \quad (3)$$

where k represents the kth order moment. Finally, higher-order absolute and central (μ_k) kth-order moments were calculated as

$$\mu_k = \int_0^{t_{max}} C_{norm}(t)\,(t - M_1)^k\,dt \quad (4)$$

The zeroth moment (M_0) is, by definition, unity for the normalized time series. The first moment (M_1) represents the mean arrival time of the observed signal. The second central moment (μ_2) describes the temporal spreading of the signal as it passes an observation point. The third central moment (μ_3) describes asymmetry of the time series, and can be used to calculate skewness (γ):

$$\gamma = \frac{\mu_3}{\mu_2^{3/2}} \quad (5)$$

Results

Solute Tracer and Electrical Resistivity Tomography

Specific conductivity of the stream increased from 228 µS/cm at baseline to 368 µS/cm during the tracer plateau. Specific conductivity in the pore water increased from 223 to 348 µS/cm at the cross-vane and 230 to 343 µS/cm at the riffle. The tracer arrived at the cross-vane piezometer rapidly, reaching plateau approximately 8 min after the stream (Figure 2A). At the riffle, the tracer arrival was slower, reaching plateau approximately 48 min after

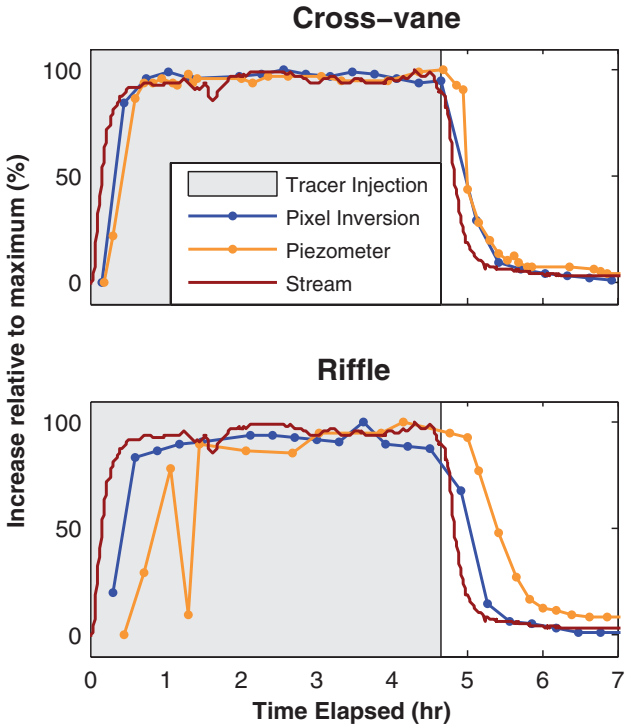

Figure 2. Time series of fluid conductivity for the stream and piezometers, and bulk electrical conductivity for the inversion pixels that correspond spatially to the piezometer screen. Conductivity measurements correlate strongly between each method suggesting confidence in our data collecting techniques.

the stream (Figure 2B). Electrical resistivity values shown in Figure 2 are based on the single pixel centered nearest to the middle of the screened section of the piezometer.

The resolution of the inversion was greatest near the surface and centered on the stream channel decreasing with depth from the ground surface and near the edges of the transect (Figure 3A and 3B). Pre-tracer electrical resistivity ranged from 90 to 410 Ω-m (Figure 3C and 3D), and pixel time series were inverted compared to corresponding pre-tracer values. We interpret neither discernable lithological boundaries nor notable features in pre-tracer resistivity. The maximum bulk electrical conductivity (minimum bulk electrical resistivity) observed at each pixel is presented in Figure 3E and 3F. Notably, several pixels located well away from the stream channel meet our clipping thresholds of resolution and minimum change from background at the riffle (pixels at $X > 20$ m in the right-hand column of plots in Figure 3) for only one time step. Figure 2 presents the conductivity time series for the stream, piezometers, and the ER pixel that is spatially co-located with the piezometer screen. The maximum cross-sectional hyporheic areas, interpreted from the pixels passing our thresholds for both resolution and peak decrease in bulk electrical resistivity, were 10.2 and 11.1 m^2 for the cross-vane and riffle, respectively (Figure 4). Hyporheic flowpaths labeled with the tracer rapidly reached a plateau at both structures and flushed within approximately 0.5 h of the injection ending (Figure 4).

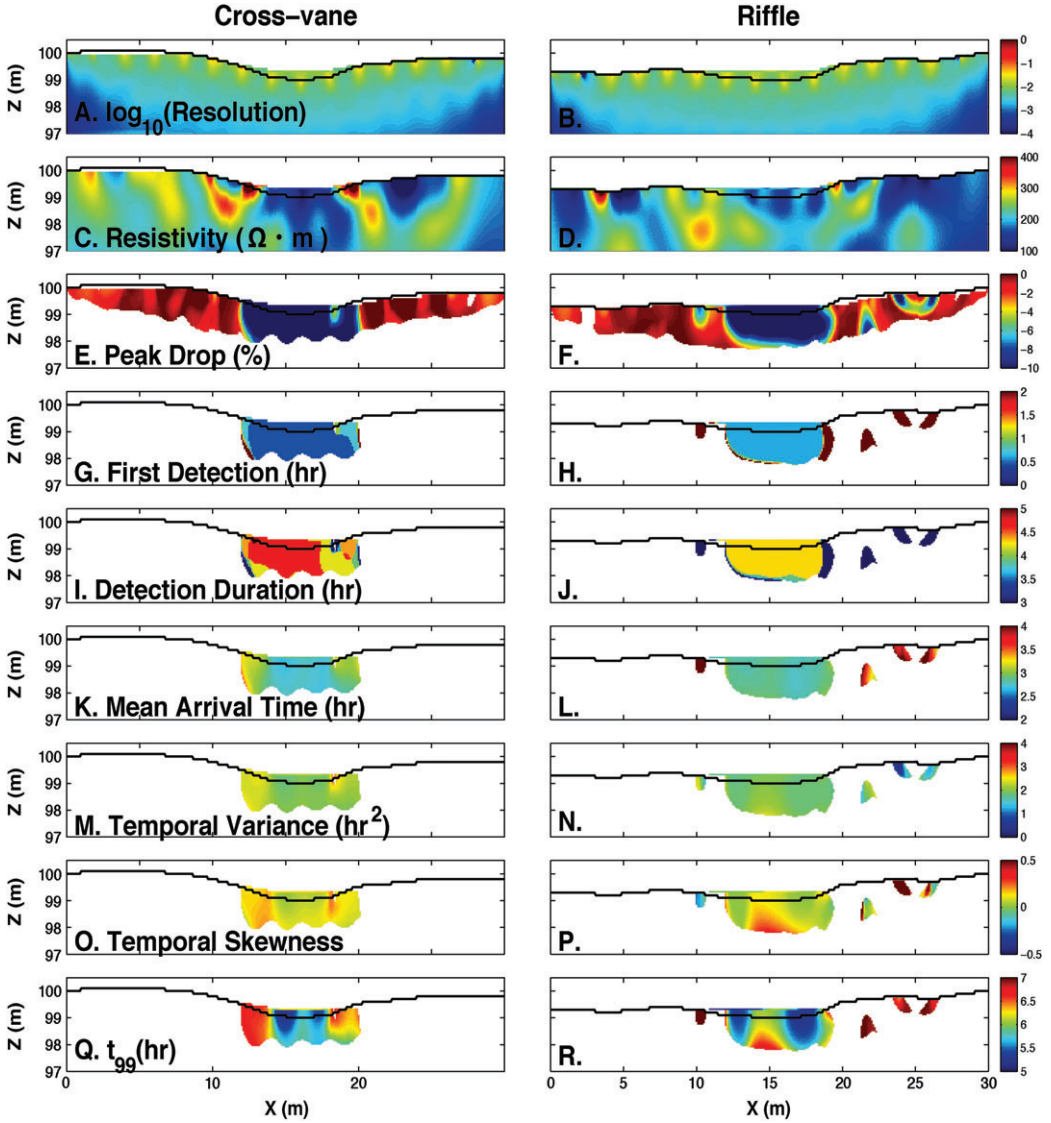

Figure 3. ER images conceptualize hyporheic extent and transport. In each panel, the river is represented by the colored area above the streambed (black line). For each transect (columns), images show (A and B) resolution of the geophysical inversion, (C and D) pre-tracer, or background, electrical resistivity, (E and F) peak decrease in bulk electrical resistivity from pre-tracer observations, (G and H) first detection (t_{first}, the time a pixel first detected tracer at a level of more than 5% from background), (I and J) detection duration ($t_{detection}$, time elapsed between first and last detections), (K and L) mean arrival time (M_1, the mean transit time of tracer from the injection to the transect), (M and N) temporal variance of the tracer signal (μ_2), (O and P) skewness of the tracer signal (γ), and (Q and R) t_{99} (the time at which 99% of the observed tracer signal passed a pixel).

Time-Series Analysis of Geophysical Results

First detection (t_{first}) of tracer below each structure was rapid with median values of approximately 0.4 and 0.6 h after tracer injection for the cross-vane and riffle, respectively (Figure 3G and 3H; Table 1). The riffle is located about 18 m downstream of the cross-vane which represents an expected lag of about 0.1 h given the average in-stream velocity upstream of the cross-vane estimated using the known reach length from the injection point to the in-stream fluid conductivity logger divided by the transit time of the rising limb. The duration of detection ($t_{detection}$) averaged 4.4 h at the cross-vane and 3.3 h at the riffle (Figure 3I and 3J; Table 1). Mean arrival time (M_1) averaged 2.8 and 2.9 h at the cross-vane and riffle, respectively (Figure 3K and 3L; Table 1). Temporal variance (μ_2) of flowpaths was larger in the cross-vane than in the natural riffle, with mean values 2.1 and 1.9 h^2 for the cross-vane and riffle, respectively (Figure 3M and 3N; Table 1). Greater temporal skewness (γ) occurred at the natural riffle than at the cross-vane (average values of 0.16 and 0.11, respectively). Average t_{99} value for both the cross-vane and riffle was 6.0 h (Figure 3O and 3P; Table 1). Summary statistics for the time-series analyses are presented in Table 1.

Average values of mean arrival time (M_1) and temporal variance (μ_2) from the electrical resistivity data were comparable to the fluid specific conductivity values in the piezometers for the cross-vane (Figure 2).

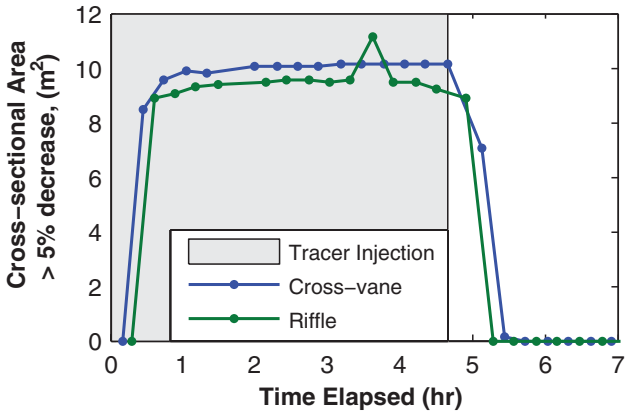

Figure 4. Apparent hyporheic cross-sectional area rapidly reached peak values at each feature. The cross-vane hyporheic zone is 12% larger in spatial extent compared to the riffle. At both features, tracer was quickly flushed from the hyporheic zone.

Piezometers represent a limited suite of flowpaths that intersect the piezometer screen while results of ER measurements aggregate the solute transport effects of a larger number of flowpaths. Comparison of the two (Table 1) provides information about the rapid exchanges occurring near the stream centerline (i.e., the piezometer) with the bulk metrics of the entire hyporheic zone (i.e., the ER data). The average ER-derived mean arrival time (M_1) and temporal variance (μ_2) were smaller than the piezometers for the riffle. Average skewness (γ) based on ER was smaller than that observed in the piezometers. Average first arrival time (t_{first}) in the ER data was slower than in the piezometers. Detection duration ($t_{detection}$) and last detection were also shorter in the ER data compared to the stream. These disparities represent a combination of spatial scale of integration (i.e., a single point at the piezometer as compared to a field of measurements in the ER images) and the potential for the chosen threshold of 5% change to effect interpretations (i.e., earlier arrival and later departure may have been sensed using a lower threshold, which would also increase temporal variance [μ_2] and skewness [γ]). This comparison highlights the complexity of hyporheic flowpaths and the need for spatially extensive characterizations to quantify the distribution of hyporheic timescales and processes.

To visualize differences between the cross-vane and the riffle, we constructed cumulative distribution functions of pixel populations for each metric at each transect (Figure 5). At the cross-vane, rapid mean arrival (M_1) of the tracer was faster than that of the riffle; the cross-vane also had fewer pixels with late-time persistence compared to the riffle (Figure 5A). Temporal variance (μ_2) of tracer pulse was primarily distributed over the range of 1.7 to 2.5 h^2 for both structures (Figure 5B). Most pixels were positively skewed at both transects, though about 5% of pixels at the riffle had a negative skew (Figure 5C). The riffle had a larger fraction of pixels that were more highly skewed than the restoration structure (Figure 5C). First detection (t_{first}) at the cross-vane was more rapid than at the riffle. At the riffle, about 22% of pixels had a

Table 1
Time-Series Metrics for Observed In-Stream Fluid Conductivity, Piezometer Fluid Conductivity, and Electrical Resistivity Images

Fluid Specific Conductivity				ER Summary Statistics		
	Stream	Cross-Vane	Riffle	Parameter	Cross-Vane	Riffle
M_1 (h)	2.7	2.9	3.4	Mean Median St. Dev.	2.9 2.8 0.2	3.0 2.9 0.4
μ_2 (h^2)	2.2	2.2	2.2	Mean Median St. Dev.	2.1 2.0 0.2	1.9 1.9 0.3
γ	0.3	0.3	0.2	Mean Median St. Dev.	0.1 0.1 0.0	0.2 0.8 0.4
t_{first} (h)	0.4	0.2	0.5	Mean Median St. Dev.	0.6 0.5 0.4	1.3 0.6 0.4
t_{99} (h)	6.6	6.7	7.3	Mean Median St. Dev.	6.1 6.1 0.4	6.0 6.0 0.5
$t_{detection}$ (h)	6.2	6.5	6.9	Mean Median St. Dev.	4.4 4.7 0.7	3.3 4.3 1.8

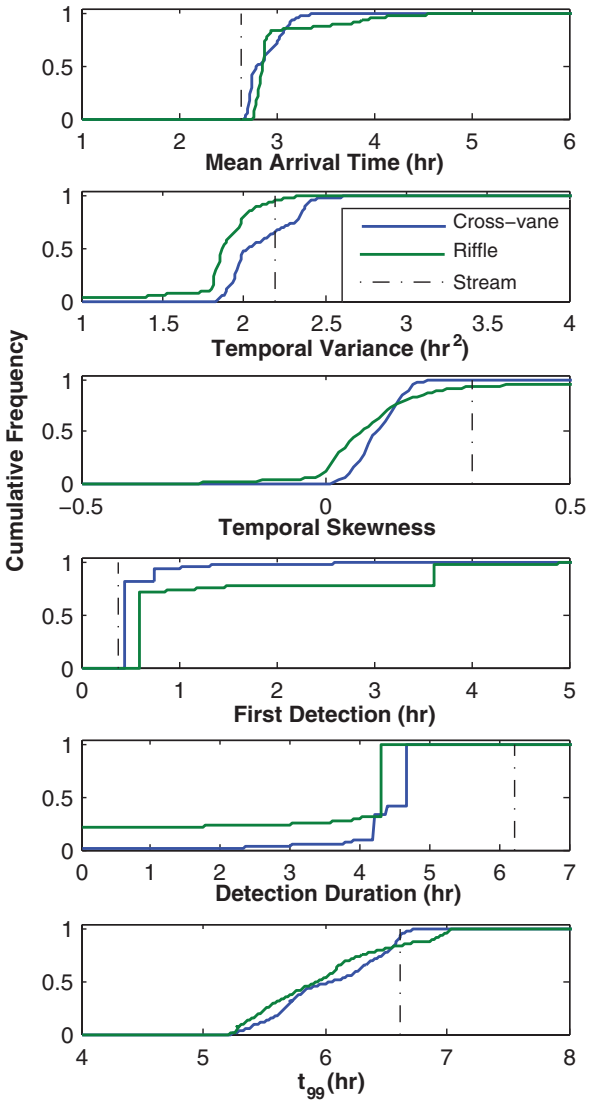

Figure 5. Cumulative distribution functions graphically quantify pixel time series in response to passing tracer depicted in ER images. For example, nearly 80% of pixels at the cross-vane first encountered tracer at 0.45 h, and 70% of pixels at the riffle first encountered tracer at 0.55 h. Observed stream metrics compare surface water patterns to those in the hyporheic zone.

first detection (t_{first}) at approximately 3.7 h (Figure 5D), mostly associated with the anomalous pixels near $X = 25$ m. Detection of duration ($t_{\text{detection}}$) at the riffle included about 23% of pixels detected for zero duration (i.e., for a single time step; Figure 5E, again corresponding to the anomalous pixels near $X = 25$ m). Time to 99% of signal detection (t_{99}) was similar between the two transects with a more uniform t_{99} at the cross-vane (Figure 5F).

Discussion

Hyporheic Transport Is Heterogeneous at and Between Structures

The results of this study demonstrate a high degree of variability in the hyporheic transport metrics both at the individual transects and comparing between transects. At the cross-vane, the flowpaths directly below the streambed and near the stream are characterized by rapid first detection (t_{first}), short mean arrival time (M_1), short t_{99}, and long duration of detection. These flowpaths are fairly uniform in space over an apparent area of approximately 8 m^2, based on spatial patterns in transport metrics (Figure 3). In contrast, flowpaths located near the edges of the hyporheic extent have longer time elapsed to first detection (t_{first}), longer mean arrival time (M_1), and longer t_{99}. However, these flowpaths travel faster through the exchange zone as evidenced by shorter detection duration ($t_{\text{detection}}$). They are also more temporally heterogeneous as evidenced by greater temporal variance (μ_2) and skewness (γ). When compared to the cross-vane, the riffle showed similar transport patterns directly beneath the streambed and near the stream as characterized by quick first detection (t_{first}), short mean arrival (M_1), and long detection duration. However, the riffle showed greater heterogeneity throughout the entirety of the exchange zone as characterized by greater skewness (γ) and longer t_{99}.

The two study transects were located in contrasting in-stream features with the upstream transect at a recently installed cross-vane and the downstream transect at a riffle. Transport patterns at the cross-vane have characteristically divided behavior based on flowpath location in the hyporheic zone. For example, first detection (t_{first}) was either within the first hour (directly below the streambed and near the stream) or after 2 h (the edge of the hyporheic zone). In contrast, transport at the riffle is better characterized by gradients from rapid to slower first detection (t_{first}) throughout the exchange zone. We hypothesize the homogeneity in behavior at the cross-vane (excluding the edge of the hyporheic zone) can be attributed to a well-sorted, open-matrix backfill behind the cross-vane during construction. This both homogenizes soil properties and allows for rapid, extensive downwelling of stream water. In contrast, transport at the riffle reflects that of a poorly sorted porous media with longer transport timescales. Deeper flowpaths directly beneath the riffle are more highly skewed and have longer t_{99} compared to the cross-vane. As hyporheic flowpaths at the riffle travel through the subsurface, changes in bed material drive variances in flowpath patterns. This is not seen at the cross-vane due to the recent construction of the structure where backfill is a cobble and gravel substrate reaching more than 1 m into the subsurface (Daniluk et al. 2013). The preceding results demonstrate that these geomorphologic features contrast in hyporheic transport patterns. Based on these patterns, we infer heterogeneity in the biogeochemical processes would also be present.

The result of this study must be interpreted within the context of the study design, which included two primary limitations. First, our study design is limited in sample size, with only one riffle and cross-vane having been studied. This requires the inherent assumption that these structures are comparable and that variability in transport patterns is due to structure design and not natural variability. Based on their geometries, geological and

hydrological setting, and the head drop across the structures, we argue a comparison is valid. The study with the largest sample population in the literature compared vertical hydraulic gradient, water surface concavity, and streambed length in up- or downwelling to geomorphologic metrics (Anderson et al. 2005; Gooseff et al. 2006), but did not characterize transport at individual features. Kasahara and Wondzell (2003) studied reaches with several riffle or step features, but did not quantify transport at the scale of individual features, focusing instead on reach-integrated behavior. Additionally, Kasahara and Hill (2006) concluded that constructed riffles encourage greater vertical surface water-groundwater linkage than natural riffles but did not quantify variability between groups. To the best of our knowledge, no studies have been conducted comparing transport variability between enough riffles to quantify within-group or between-group variability as a function of morphology. Our study is one of the first to attempt comparison of hyporheic transport at natural features and restoration structures using a spatially distributed characterization of transport processes. Our assumption that the cross-vane and riffle can be directly compared parallels the efforts of Kasahara and Hill (2006) who found hyporheic exchange flow induced by a constructed step was consistent with natural steps. Kasahara and Hill (2006) also found that constructed riffles create more hyporheic exchange flux than natural riffles, further supporting our hypothesis that anthropogenic features are capable of inducing exchange flux at magnitudes larger than natural features. Future study of multiple riffles and cross-vanes could help contextualize within-group and between-group variability and also performance under different hydrological conditions.

A second complication in our study is the potential impact of the upstream structure on the downstream feature, since the two are in series along a stream. The proximity of the restoration structure and the natural riffle limits differences due to larger-scale geological controls and hydrological drivers of hyporheic exchange (Larkin and Sharp 1992; Ward et al. 2012a; Wondzell and Gooseff 2013). Geological and hydrological differences between reference sites and restored sites could vary widely, limiting our ability to compare behavior or individual structures or features as a key variable of interest. Indeed, Daniluk et al. (2013) noted several limitations in comparing reference and restored reaches, including the fairness of a comparison of sites that have been differentially impacted by construction activities.

Study of consecutive features, as in our field experiment, is limited by the potential for the interaction of the two features. In our study, flowpaths at the cross-vane with residence times within the tracer study window of detection (sensu Harvey et al. 1996; Ward et al. 2013b) would affect the in-stream tracer signal arriving at downwelling flowpaths at the riffle. The hyporheic flow field at consecutive features has not been studied as a direct function of morphology or feature spacing. No literature studies provide guidance of the spatial window of influence that an individual feature has on subsequent, downgradient features in the stream. Published results generally show the shortest and fastest flowpaths at each feature are driven by the feature itself, while the longer timescale and deeper flowpaths are more likely affected by multiple features (e.g., Figure 2 in Gooseff et al. 2006 and Figure 3 in Ward et al. 2013a). We assume the tracer-labeled hyporheic zones at the consecutive features are independent due to the channel-spanning upwelling zone between the two downwelling locations (Figure 1B).

In addition to interaction of the physical flowpaths, the serial interactions along the stream must also consider the solute tracer signal at each downwelling flowpath location. Specifically, the fluid conductivity output from the cross-vane and its plunge pool provide the input to the downstream riffle. In practice, the use of a whole-stream tracer study to deliver a replicate input signal to the cross-vane and riffle is not possible. The input signal of each is uniquely influenced by the transport processes being aggregated between the tracer input location and the ER transect. For the downstream riffle, this includes the impact of the upstream cross-vane and the associated hyporheic zone, in-stream dead zones, and plunge pool. In our study, we expect the superposition of cross-vane tracer outflow to riffle inflow would be most pronounced during late times, when both in-channel and hyporheic temporary storage of the tracer at the cross-vane and plunge pool may contribute an increased late-time, in-stream tracer concentration at downwelling riffle flowpaths. The use of t_{99} as a late-time metric and to truncate the time series being analyzed excludes the latest-time interactions of the cross-vane hyporheic flowpaths contributing to the downwelling tracer signal at the riffle, though we acknowledge that interaction throughout the time series is inevitable in our study design. If the cross-vane had a significant impact on the in-stream solute tracer time series downwelling at the riffle, we would expect differences in temporal variance (indicating longitudinal spreading of the signal in the stream) and skewness (indicating exchange with locations outside of the advection-dominated flow) in the fluid conductivity time series observed at each site. In our study, the fluid conductivity time series at the cross-vane and the riffle had identical μ_2 and reduced γ at the riffle, suggesting that the cross-vane had a minimal impact on the solute tracer time series that arrived at the riffle.

Contrasting Interpretations and Implications for Restoration Design

This site has previously been investigated using both biogeochemical analysis of pore water and vertical temperature profiles by Gordon et al. (2013). Based on the rapid vertical up- and downwelling observed through the temperature profiles, Gordon et al. (2013) concluded that the cross-vane created shorter residence-time hyporheic flowpaths than the riffle. Based on pore water chemistry showing no NO_3^- production and reduced redox chemistry variation, Gordon et al. (2013) further concluded that the cross-vane was significantly less important to the stream ecosystem than the riffle.

However, our study demonstrates the presence of some longer transit-time hyporheic flowpaths at the cross-vane than at the riffle.

The contrasting interpretations can be explained by the limitations of each method, specifically the spatial orientation of flowpaths to which the methods are sensitive and the spatial domain investigated. First, Gordon et al. (2013) estimated fluxes across the streambed in the vertical dimension using one-dimensional (1D) temperature profiles. The interpretation of temperature signal attenuation in the vertical dimension isolates only the vertical component of the flowpaths. This is a recognized limitation of the method, though 2D and 3D patterns are inferred in some studies (e.g., Briggs et al. 2012). Indeed, we concur with Gordon et al.'s (2013) interpretation of rapid downwelling at the cross-vane to be greater than at the riffle as evidenced by rapid first-arrival times at that structure (Figure 5). ER images are not directly sensitive to vertical fluxes; rather, they are sensitive to flowpaths that intersect the imaging plane regardless of their orientation. Furthermore, the spatial extent of study by Gordon et al. (2013) is more limited than the extent of ER. The biogeochemical analyses of Gordon et al. (2013) quantified hyporheic exchange less than 20 cm from the surface at each feature. It is possible that optimal depth for biogeochemical processing at the cross-vane is greater than 20 cm, where 20 cm depth may be ideal for processing at the riffle. Given sensitivity to differing spatial domains and flux orientations, the two techniques are complimentary in their assessment of hyporheic transport but must be interpreted as such (i.e., each tells a portion of the story, but capture some unique dynamics).

It has been suggested, in the context of hyporheic restoration, that ecosystem function follows form (i.e., greater hyporheic exchange flux will result in greater ecosystem process; Findlay 1995; Boulton 2007; Ward et al. 2012a). However, results of our study challenge this philosophy. Gordon et al. (2013) concluded that the lack in biogeochemical processing at the cross-vane was due to the decreased hyporheic residence time; we found first arrival and duration of detection to be longer at the cross-vane. Given the biogeochemical interpretation of Gordon et al. (2013), we interpret the biogeochemical processing at the cross-vane as limited despite increased persistence. For example, the constructed cross-vane may not support the same microbial community as the riffle due to increased exchange flux. This interpretation agrees with Zimmer and Lautz (in press), who conclude that too large rates of hyporheic transport can ultimately limit the ecological benefits of a stream feature and supports Harvey and Fuller (1998) who concluded the biogeochemical benefits of hyporheic exchange are a direct function of the relationship between timescales and length scales of hyporheic flowpaths. The notion that biogeochemical processing increases with depth at the cross-vane could support the concept that function follows form if that function occurs at greater depths with larger exchange zones.

Hyporheic restoration must consider a balance of physical transport and biogeochemical processes. Previous studies have demonstrated that this balance can be engineered to achieve desired services. For example, van Driel et al. (2006) and Robertson and Merkley (2009) added woodchips, a source of organic carbon, to their bioreactors to achieve denitrification of agricultural runoff, their desired ecological function. Their work demonstrates that engineering of both physical and biogeochemical conditions can be achieved and shows promise for engineered hyporheic zones as a water quality management practice. However, our study in comparison to Gordon et al. (2013) demonstrates the importance of thoroughly understanding the balance of physical and temporal flowpaths and the resulting biogeochemical processes before structure design can be implemented as an accepted restoration technique.

Apart from the preceding discussions, several additional techniques do exist that serve as complimentary methods for better interpreting both the physical and chemical components of hyporheic exchange. For example, the physical transport of hyporheic flowpaths have been quantified by techniques such as surface and subsurface temperature profiles (e.g., Vogt et al. 2010; Briggs et al. 2012), flux measurement across streambeds (e.g., Cardenas et al. 2004; Salehin et al. 2004), and pressure distribution throughout a reach (e.g., Packman et al. 2004; Tonina and Buffington 2007). Biogeochemical processes have been quantified using techniques such as pore water sampling (e.g., McKnight et al. 2004; Fischer et al. 2005) and chemically reactive tracers (e.g., Haggerty et al. 2008; Lemke et al. 2013). Using complimentary methods would better address confidence in our understanding of physical transport at natural and anthropogenic features.

Conclusions

In recent years, several studies have promoted hyporheic restoration as a design goal for stream restoration projects (e.g., Palmer and Bernhardt 2006; Bernhardt and Palmer 2007; Boulton 2007; Boulton et al. 2010; Hester and Gooseff 2010, 2011; Krause et al. 2011). Challenges to the inclusion of hyporheic exchange as a restoration goal include the lack of predictive power regarding the potential for designed structures to create hyporheic zones similar to natural features and a lack of common field techniques that are reliable and robust. The techniques used in this study uniquely capture the spatially distributed transport of tracer along hyporheic flowpaths in a 2D plane at resolutions unachievable by other methods and at late temporal scales other methods (e.g., stream solute modeling, vertical temperature profiling) may not quantify. To the best of our knowledge, this study is one of the first to directly compare hyporheic transport at a restoration structure and a natural feature.

We conclude that (1) hyporheic flowpath networks at the restoration structure and a natural feature in our study are different in their transport patterns; (2) the cross-vane created spatially larger and temporally longer

hyporheic flowpaths than the natural riffle at the apparent zone of peak downwelling; and (3) different methods to quantify hyporheic exchange flux and subsurface transport processes may lead to contrasting interpretations as a function of their complementary strengths and limitations. From these conclusions, we infer that restoration structures may be capable of creating high exchange flux and sufficient residence times to achieve the same ecological functions as natural features, but engineering of the biogeochemical environment may be necessary to realize these benefits. Finally, we note that metrics describing time series of solute concentrations at the piezometers are represented by the ER distributions, at least to the correct order of magnitude. Refinement of the thresholds selected and methodology could improve this representation and provide more quantitative assessment of uncertainty in the ER time-series analyses.

Acknowledgments

This article is based on work supported by the National Science Foundation's Hydrologic Sciences program, under grant nos. EAR-0911612 and EAR 0911547, and the Environmental Protection Agency's Science to Achieve Results fellowship 91737501-0. SUNY-ESF provided support for the field campaign. Any opinions, findings, and conclusions or recommendations expressed in this material are those of the authors and do not necessarily reflect the views of the National Science Foundation. The authors thank Ryan Gordon for providing the spatial data for the field site and the landowners of Luszczek Farms. We thank the editor and reviewers for comments that improved the quality of this article.

Authors' Note: The authors do not have any conflicts of interest or financial disclosures to report.

References

Anderson, J.K., S.M. Wondzell, M.N. Gooseff, and R. Haggerty. 2005. Patterns in stream longitudinal profiles and implications for hyporheic exchange flow at the H.J. Andrews Experimental Forest, Oregon, USA. *Hydrological Processes* 19, no. 15: 2931–2949.

Battin, T.J. 1999. Hydrologic flow paths control dissolved organic carbon fluxes and metabolism in an alpine stream hyporheic zone. *Water Resources Research* 35, no. 10: 3159–3169.

Bernhardt, E.S., and M.A. Palmer. 2007. Restoring streams in an urbanizing world. *Freshwater Biology* 52, no. 4: 738–751.

Bernhardt, E.S., M. Palmer, J. Allan, G. Alexander, K. Barnas, S. Brooks, J. Carr, S. Clayton, C. Dahm, and J. Follstad-Shah. 2005. Synthesizing U.S. river restoration efforts. *Science (Washington)* 308, no. 5722: 636–637.

Binley, A., and A. Kemna. 2005. DC resistivity and induced polarization methods. *Hydrogeophysics* 50: 129–156.

Binley, A., S. Henry-Poulter, and B. Shaw. 1996. Examination of solute transport in an undisturbed soil column using electrical resistance tomography. *Water Resources Research* 32, no. 4: 763–769.

Boulton, A.J. 2007. Hyporheic rehabilitation in rivers: Restoring vertical connectivity. *Freshwater Biology* 52, no. 4: 632–650.

Boulton, A.J., S. Findlay, P. Marmonier, E.H. Stanley, and H.M. Valett. 1998. The functional significance of the hyporheic zone in streams and rivers. *Annual Review of Ecology and Systematics* 29: 59–81.

Boulton, A.J., G.D. Fenwick, P.J. Hancock, and M.S. Harvey. 2008. Biodiversity, functional roles and ecosystem services of groundwater invertebrates. *Invertebrate Systematics* 22, no. 2: 103–116.

Boulton, A.J., T. Datry, T. Kasahara, M. Mutz, and J.A. Stanford. 2010. Ecology and management of the hyporheic zone: Stream-groundwater interactions of running waters and their floodplains. *Journal of the North American Benthological Society* 29, no. 1: 26–40.

Briggs, M.A., L.K. Lautz, J.M. McKenzie, R.P. Gordon, and D.K. Hare. 2012. Using high resolution distributed temperature sensing to quantify spatial and temporal variability in vertical hyporheic flux. *Water Resources Research* 48, no. 2: W02527. DOI:10.1029/2011WR011227.

Brunke, M., and T. Gonser. 1997. The ecological significance of exchange processes between rivers and groundwater. *Freshwater Biology* 37, no. 1: 1–33.

Cardenas, M.B., and M.S. Markowski. 2011. Geoelectrical imaging of hyporheic exchange and mixing of river water and groundwater in a large regulated river. *Environmental Science & Technology* 45, no. 4: 1407–1411.

Cardenas, M.B., J.L. Wilson, and V.A. Zlotnik. 2004. Impact of heterogeneity, bed forms, and stream curvature on subchannel hyporheic exchange. *Water Resources Research* 40, no. 8: W08307. DOI:10.1029/2004WR003008.

Craig, L.S., M.A. Palmer, D.C. Richardson, S. Filoso, E.S. Bernhardt, B.P. Bledsoe, M.W. Doyle, P.M. Groffman, B.A. Hassett, and S.S. Kaushal. 2008. Stream restoration strategies for reducing river nitrogen loads. *Frontiers in Ecology and the Environment* 6, no. 10: 529–538.

Crispell, J.K., and T.A. Endreny. 2009. Hyporheic exchange flow around constructed in-channel structures and implications for restoration design. *Hydrological Processes* 23, no. 8: 1158–1168.

Daniluk, T.L., L.K. Lautz, R.P. Gordon, and T.A. Endreny. 2013. Surface water–groundwater interaction at restored streams and associated reference reaches. *Hydrological Processes* 27, no. 25: 3730–3746.

Day-Lewis, F.D., K. Singha, and A.M. Binley. 2005. Applying petrophysical models to radar travel time and electrical resistivity tomograms: Resolution-dependent limitations. *Journal of Geophysical Research* 110, no. B8: B08206. DOI:10.1029/2004JB003569.

Day-Lewis, F.D., Y. Chen, and K. Singha. 2007. Moment inference from tomograms. *Geophysical Research Letters* 34, no. 22: L22404. DOI:10.1029/2007GL031621.

van Driel, P.W., W.D. Robertson, and W.C. Merkley. 2006. Denitrification of agricultural drainage using wood-based reactors. *Transactions of the ASCE* 49, no. 2: 565–573.

Endreny, T., and L. Lautz. 2012. Comment on 'Munz M, Krause S, Tecklenburg C, Binley A. Reducing monitoring gaps at the aquifer–river interface by modelling groundwater surfacewater exchange flow patterns'. *Hydrological Processes* 26, no. 10: 1586–1588.

Endreny, T., L. Lautz, and D. Siegel. 2011. Hyporheic flow path response to hydraulic jumps at river steps: Flume and hydrodynamic models. *Water Resources Research* 47, no. 2: W02517. DOI:10.1029/2009WR008631.

Fanelli, R.M., and L.K. Lautz. 2008. Patterns of water, heat, and solute flux through streambeds around small dams. *Groundwater* 46, no. 5: 671–687.

Fellows, C.S., H.M. Valett, and C.N. Dahm. 2001. Whole-stream metabolism in two montane streams: Contribution of the hyporheic zone. *Limnology and Oceanography* 46, no. 3: 523–531.

Findlay, S. 1995. Importance of surface-subsurface exchange in stream ecosystems: The hyporheic zone. *Limnology and Oceanography* 40, no. 1: 159–164.

Fischer, H., F. Kloep, S. Wilzcek, and M.T. Pusch. 2005. A river's liver–microbial processes within the hyporheic zone of a large lowland river. *Biogeochemistry* 76, no. 2: 349–371.

Gooseff, M.N., J.K. Anderson, S.M. Wondzell, J. LaNier, and R. Haggerty. 2006. A modelling study of hyporheic exchange pattern and the sequence, size, and spacing of stream bedforms in mountain stream networks, Oregon, USA. *Hydrological Processes* 20, no. 11: 2443–2457.

Gordon, R.P., L.K. Lautz, and T.L. Daniluk. 2013. Spatial patterns of hyporheic exchange and biogeochemical cycling around cross-vane restoration structures: Implications for stream restoration design. *Water Resources Research* 49, no. 4: 2040–2055.

Gupta, A., and V. Cvetkovic. 2002. Material transport from different sources in a network of streams through a catchment. *Water Resources Research* 38, no. 7: 3-1–3-12.

Haggerty, R., A. Argerich, and E. Martí. 2008. Development of a "smart" tracer for the assessment of microbiological activity and sediment-water interaction in natural waters: The resazurin-resorufin system. *Water Resources Research* 44, no. 4: W00D01. DOI:10.1029/2007WR006670.

Harvey, J.W., and C.C. Fuller. 1998. Effect of enhanced manganese oxidation in the hyporheic zone on basin-scale geochemical mass balance. *Water Resources Research* 34, no. 4: 623–636.

Harvey, J.W., B.J. Wagner, and K.E. Bencala. 1996. Evaluating the reliability of the stream tracer approach to characterize stream-subsurface water exchange. *Water Resources Research* 32, no. 8: 2441–2451.

Hester, E.T., and M.W. Doyle. 2008. In-stream geomorphic structures as drivers of hyporheic exchange. *Water Resources Research* 44, no. 3: W03417. DOI:10.1029/2006WR005810.

Hester, E.T., and M.N. Gooseff. 2010. Moving beyond the banks: Hyporheic restoration is fundamental to restoring ecological services and functions of streams. *Environmental Science & Technology* 44, no. 5: 1521–1525.

Hester, E.T., and M.N. Gooseff. 2011. Hyporheic restoration in streams and rivers. *Geophysical Monograph Series* 194: 167–187.

Hester, E.T., M.W. Doyle, and G.C. Poole. 2009. The influence of in-stream structures on summer water temperatures via induced hyporheic exchange. *Limnology and Oceanography* 54, no. 1: 355–367.

Kasahara, T., and A.R. Hill. 2006. Hyporheic exchange flows induced by constructed riffles and steps in lowland streams in southern Ontario, Canada. *Hydrological Processes* 20, no. 20: 4287–4305.

Kasahara, T., and S.M. Wondzell. 2003. Geomorphic controls on hyporheic exchange flow in mountain streams. *Water Resources Research* 39, no. 1: SBH3-1–SBH3-14.

Kemna, A., B. Kulessa, and H. Vereecken. 2002. Imaging and characterisation of subsurface solute transport using electrical resistivity tomography (ERT) and equivalent transport models. *Journal of Hydrology* 267, no. 4: 125–146.

Koestel, J., J. Vanderborght, M. Javaux, A. Kemna, A. Binley, and H. Vereecken. 2009. Noninvasive 3-D transport characterization in a sandy soil using ERT: 1. Investigating the validity of ERT-derived transport parameters. *Vadose Zone Journal* 8, no. 3: 711–722.

Krause, S., D. Hannah, J. Fleckenstein, C. Heppell, D. Kaeser, R. Pickup, G. Pinay, A. Robertson, and P. Wood. 2011. Interdisciplinary perspectives on processes in the hyporheic zone. *Ecohydrology* 4, no. 4: 481–499.

LaBrecque, D.J., and X. Yang. 2001. Difference inversion of ERT data: A fast inversion method for 3-D in situ monitoring. *Journal of Environmental and Engineering Geophysics* 6, no. 2: 83–89.

Larkin, R.G., and J.M. Sharp, Jr. 1992. On the relationship between river-basin geomorphology, aquifer hydraulics, and ground-water flow direction in alluvial aquifers. *Geological of Society of America Bulletin* 104, no. 12: 1608–1620.

Lautz, L.K., and R. Fanelli. 2008. Seasonal biogeochemical hotspots in the streambed around restoration structures. *Biogeochemistry* 91, no. 1: 85–104.

Lautz, L.K., and R.E. Ribaudo. 2012. Scaling up point-in-space heat tracing of seepage flux using bed temperatures as a quantitative proxy. *Hydrogeology Journal* 20, no. 7: 1223–1238.

Lemke, D., Z. Liao, T. Wöhling, K. Osenbrück, and O.A. Cirpka. 2013. Concurrent conservative and reactive tracer tests in a stream undergoing hyporheic exchange. *Water Resources Research* 49, no. 5: 3024–3037.

Mason, S.J., B.L. McGlynn, and G.C. Poole. 2012. Hydrologic response to channel reconfiguration on Silver Bow Creek, Montana. *Journal of Hydrology* 438: 125–136.

McKnight, D.M., R.L. Runkel, C.M. Tate, J.H. Duff, and D.L. Moorhead. 2004. Inorganic N and P dynamics of Antarctic glacial meltwater streams as controlled by hyporheic exchange and benthic autotrophic communities. *Journal of the North American Benthological Society* 23, no. 2: 171–188.

Menichino, G.T., A.S. Ward, and E.T. Hester. 2014. Macropores as preferential flow paths in meander bends. *Hydrological Processes* 28, no. 3: 482–495.

Nyquist, J.E., L. Toran, A.C. Fang, R.J. Ryan, and D.O. Rosenberry. 2010. Tracking tracer breakthrough in the hyporheic zone using time-lapse DC resistivity, Crabby Creek, Pennsylvania. In *Proceedings of the Annual Symposium on the Application of Geophysics to Engineering and Environmental Problems*, March 11–15, Denver, Colorado. Environmental and Engineering Geophysical Society.

Packman, A.I., M. Salehin, and M. Zaramella. 2004. Hyporheic exchange with gravel beds: Basic hydrodynamic interactions and bedform-induced advective flows. *Journal of Hydraulic Engineering* 130, no. 7: 647–656.

Palmer, M.A., and E.S. Bernhardt. 2006. Hydroecology and river restoration: Ripe for research and synthesis. *Water Resources Research* 42, no. 3: W03S07. DOI:10.1029/2005WR004354.

Pinay, G., T.C. O'Keefe, R.T. Edwards, and R.J. Naiman. 2009. Nitrate removal in the hyporheic zone of a salmon river in Alaska. *River Research and Applications* 25, no. 4: 367–375.

Robertson, W.D., and L.C. Merkley. 2009. In-stream bioreactor for agricultural nitrate treatment. *Journal of Environmental Quality* 38, no. 1: 230–237.

Salehin, M., A.I. Packman, and M. Paradis. 2004. Hyporheic exchange with heterogeneous streambeds: Laboratory experiments and modeling. *Water Resources Research* 40, no. 11: W11504. DOI:10.1029/2003WR002567.

Sawyer, A.H., and M.B. Cardenas. 2012. Hyporheic temperature dynamics and heat exchange near channel-spanning logs. *Water Resources Research* 48, no. 1: W01529. DOI:10.1029/2011WR011200.

Sawyer, A.H., M.B. Cardenas, and J. Buttles. 2011. Hyporheic exchange due to channel spanning logs. *Water Resources Research* 47, no. 8: W08502. DOI:10.1029/2011WR010484.

Schmid, B.H. 2003. Temporal moments routing in streams and rivers with transient storage. *Advances in Water Resources* 26, no. 9: 1021–1027.

Slater, L., A. Binley, W. Daily, and R. Johnson. 2000. Cross-hole electrical imaging of a controlled saline tracer injection. *Journal of Applied Geophysics* 44, no. 2: 85–102.

Slater, L., A. Binley, R. Versteeg, G. Cassiani, R. Birken, and S. Sandberg. 2002. A 3D ERT study of solute transport in a large experimental tank. *Journal of Applied Geophysics* 49, no. 4: 211–229.

Tonina, D., and J.M. Buffington. 2007. Hyporheic exchange in gravel bed rivers with pool-riffle morphology: Laboratory experiments and three-dimensional modeling. *Water Resources Research* 43, no. 1: W01421. DOI:10.1029/2005WR004328.

Toran, L., B. Hughes, J. Nyquist, and R. Ryan. 2012. Using hydrogeophysics to monitor change in hyporheic flow around stream restoration structures. *Environmental & Engineering Geoscience* 18, no. 1: 83–97.

Valett, H.M., J.A. Morrice, C.N. Dahm, and M.E. Campana. 1996. Parent lithology, surface groundwater exchange, and nitrate retention in headwater streams. *Limnology and Oceanography* 41, no. 2: 333–345.

Vaux, W.G. 1968. Intragravel flow and interchange of water in a streambed. *Fishery Bulletin* 66, no. 3: 479.

Vidon, P., C. Allan, D. Burns, T.P. Duval, N. Gurwick, S. Inamdar, R. Lowrance, J. Okay, D. Scott, and S. Sebestyen. 2010. Hot spots and hot moments in riparian zones: Potential for improved water quality management. *Journal of the American Water Resources Association* 46, no. 2: 278–298.

Vogt, T., P. Schneider, L. Hahn-Woernle, and O.A. Cirpka. 2010. Estimation of seepage rates in a losing stream by means of fiber-optic high-resolution vertical temperature profiling. *Journal of Hydrology* 380, no. 1: 154–164.

Ward, A.S., M.N. Gooseff, and K. Singha. 2010. Imaging hyporheic zone solute transport using electrical resistivity. *Hydrological Processes* 24, no. 7: 948–953.

Ward, A.S., M.N. Gooseff, and P.A. Johnson. 2011. How can subsurface modifications to hydraulic conductivity be designed as stream restoration structures? Analysis of Vaux's conceptual models to enhance hyporheic exchange. *Water Resources Research* 47, no. 8: W08512. DOI:10.1029/2010WR010028.

Ward, A.S., M. Fitzgerald, M.N. Gooseff, T.J. Voltz, A.M. Binley, and K. Singha. 2012a. Hydrologic and geomorphic controls on hyporheic exchange during base flow recession in a headwater mountain stream. *Water Resources Research* 48, no. 4: W04513. DOI:10.1029/2011WR011461.

Ward, A.S., M. Fitzgerald, M.N. Gooseff, T.J. Voltz, A.M. Binley, and K. Singha. 2012b. Correction to "Hydrologic and geomorphic controls on hyporheic exchange during baseflow recession in a headwater mountain stream." *Water Resources Research* 48, no. 8: W08903. DOI:10.1029/2012WR012663.

Ward, A.S., M.N. Gooseff, and K. Singha. 2013a. How does subsurface characterization affect simulations of hyporheic exchange? *Groundwater* 51, no. 1: 14–28.

Ward, A.S., R.A. Payn, M.N. Gooseff, B.L. McGlynn, K.E. Bencala, C.A. Kelleher, S.M. Wondzell, and T. Wagener. 2013b. Variations in surface water-ground water interactions along a headwater mountain stream: Comparisons between transient storage and water balance analyses. *Water Resources Research* 49, no. 6: 3359–3374.

Ward, A.S., M.N. Gooseff, M. Fitzgerald, T.J. Voltz, and K. Singha. 2014. Spatially distributed characterization of hyporheic solute transport during baseflow recession in a headwater mountain stream. *Journal of Hydrology* 517: 362–377. DOI:10.1016/j.hydrol.2014.05.036.

Wondzell, S.M., and M.N. Gooseff. 2013. Geomorphic controls on hyporheic exchange across scales: Watersheds to particles. In *Treatise on Geomorphology*, ed. J. Schroder Jr. and E. Wohl, Vol. 9, 209–218. San Diego, California: Academic.

Zhou, T., and T.A. Endreny. 2013. Reshaping of the hyporheic zone beneath river restoration structures: Flume and hydrodynamic experiments. *Water Resources Research* 49, no. 8: 5009–5020.

Zimmer, M., and L. Lautz. In press. Pre- and post-restoration assessment of stream-ground water interactions: Impacts on hydrological and chemical heterogeneity in the hyporheic zone. *Freshwater Science*.